Physica E 173 (2025) 116316

Contents lists available at ScienceDirect

Physica E: Low-dimensional Systems and Nanostructures

journal homepage: www.elsevier.com/locate/physe

From 2D to 1D in β-naphthyne: A porous carbon allotrope merging graphyne and naphthylene

José A.S. Laranjeira [a,*], K.A.L. Lima [b,c], Nicolas F. Martins [a], Marcelo L.P. Junior [d], L.A. Ribeiro Junior [b,c], Julio R. Sambrano [a,*]

[a] Modeling and Molecular Simulation Group, São Paulo State University (UNESP), School of Sciences, Bauru, 17033-360, SP, Brazil
[b] Institute of Physics, University of Brasília, Brasília, 70910-900, DF, Brazil
[c] Computational Materials Laboratory, LCCMat, Institute of Physics, University of Brasília, Brasília, 70910-900, DF, Brazil
[d] University of Brasília, College of Technology, Department of Electrical Engineering, Brasília, 70910-900, DF, Brazil

ARTICLE INFO

Editor: M.W. Wu

Keywords:
Two-dimensional carbon allotrope
β-naphthyne
Density functional theory
Graphyne
Naphthylene

ABSTRACT

Two-dimensional (2D) carbon-based materials have attracted considerable interest due to their diverse structural and electronic properties, making them ideal for next-generation flat electronics. Among these materials, metallic-like porous structures offer advantages such as tunable charge transport and high surface area, which are essential for energy storage applications. In this study, we introduce β-naphthyne, a novel 2D carbon allotrope composed of naphthyl units interconnected by octagonal rings. First-principles calculations confirm its dynamic and thermal stability, demonstrating its theoretical feasibility. Furthermore, we demonstrate that Young's modulus ranges from 43.71 N/m to 165.88 N/m, indicating an anisotropic mechanical response. Optical analysis reveals absorption activity in the infrared (IR) and ultraviolet (UV) regions. The derived 1D structures were also analyzed, revealing a Dirac cone and a transition from metallic to semiconducting behavior. These findings establish β-naphthyne as a promising material for energy storage and optoelectronic technologies.

1. Introduction

Two-dimensional (2D) carbon-based materials have garnered significant attention due to their mechanical, electronic, and optical properties, making them promising candidates for energy storage and nanoelectronics applications [1–4]. Among them, porous 2D carbon allotropes offer additional advantages while maintaining a high surface-to-volume ratio, exhibiting tunable electronic structures and enhanced ion diffusion, which are crucial for hydrogen storage, supercapacitors, and metal-ion batteries [5–9]. Incorporation of ordered nanopores into carbon frameworks can introduce different electronic properties, such as Dirac cone semimetallicity, which pave the way for the development of high-performance energy materials [10–12].

Several porous carbon allotropes have been synthesized or theoretically predicted in recent years, each exhibiting distinct structural and electronic characteristics [13–17]. For instance, graphdiyne, a synthesized material featuring acetylenic linkages, exhibits enhanced electrochemical performance due to its high charge carrier mobility and tunable band gap [18]. Other experimentally synthesized materials include the biphenylene network, which was recently fabricated via on-surface synthesis and displays metallic behavior, holding potential for nanoelectronic applications [19]. In contrast, several computationally predicted structures [20–28] have been characterized, revealing distinct structural, electronic, optical, and mechanical properties. However, the experimental realization of some of these structures remains a challenge [29]. However, theoretical studies are essential for guiding experimental synthesis by predicting stability, mechanical response, and electronic characteristics, enabling researchers to design novel materials with desirable functionalities before fabrication [30,31].

Building upon recent advances in 2D carbon-based materials for surface electronics, we introduce the graphyne-like β-naphthylene (β-naphthyne) as a novel porous 2D carbon allotrope characterized by naphthalene molecules covalently linked through acetylenic groups at all their dehydrogenated terminations, forming a rectangular symmetry. β-naphthyne is a graphyne-like version of β-naphthylene, previously proposed by Paz et al. [32] in which the allotrope is predicted from the naphthalene precursor in its so-called β phase, configuring a 2D carbon allotrope with 4-, 6-, and 10-membered rings. In the structure proposed here, the linkage between naphthalene molecules is replaced by acetylenic groups, transforming the originally sp^2-bonded system into a hybrid sp-sp^2 configuration, now exhibiting 6- and

* Corresponding authors.
E-mail addresses: jose.laranjeira@unesp.br (J.A.S. Laranjeira), jr.sambrano@unesp.br (J.R. Sambrano).

https://doi.org/10.1016/j.physe.2025.116316
Received 9 March 2025; Received in revised form 7 June 2025; Accepted 14 June 2025
Available online 7 July 2025

8-membered rings, along with nanopores consisting of 18 carbon-membered units.

Regarding the challenges of synthesizing such materials, naphthalene units no longer serve as a precursor for a potential synthesis of β-naphthyne. Instead, octamethylnaphthalene ($C_{18}H_{24}$), synthesized in 1972 by Hart and Oku [33], emerges as a viable structural building block for bottom-up synthesis strategies, such as surface-assisted polymerization or templated chemical vapor deposition (CVD), providing a feasible route for future syntheses of β-naphthyne [34–36].

This study presents the novel β-naphthyne structure, investigated through first-principles calculations. Using density functional theory (DFT), we explored its electronic properties, including band structures, electron localization function (ELF), and Bader charge distribution. The thermal and dynamic stabilities were verified using *ab initio* molecular dynamics (AIMD) and phonon dispersion, respectively. A comprehensive mechanical evaluation was conducted by analyzing elastic constants, with stability confirmed via the Born-Huang criteria. In addition, the effect of 1D confinement was evaluated by analysis of β-naphthyne nanoribbons. The findings reported here not only highlight the β-naphthyne as a 2D reliable carbon allotrope but also suggest its potential as a platform for diverse applications, such as energy storage, gas detection, and electronics.

2. Methodology

To explore the structural, electronic, mechanical, and optical properties of β-naphthyne, we conducted first-principles simulations based on DFT [37]. The computational framework was implemented using the Vienna Ab Initio Simulation Package (VASP) [38]. For electron exchange and correlation effects, we employed the generalized gradient approximation (GGA) following the Perdew–Burke–Ernzerhof (PBE) functional [39]. The interaction between valence and core electrons was treated using the projector-augmented wave (PAW) method [40].

The kinetic energy cutoff for the plane-wave basis set was set to 520 eV, ensuring an accurate representation of electronic states. The structural optimizations were performed using the conjugate gradient method until the force on each atom was lower than 0.01 eV/Å, and the total energy change between successive steps was below 10^{-5} eV. A vacuum spacing of 15 Å along the out-of-plane direction was introduced to prevent interactions between periodic images. The Brillouin zone was sampled using a Γ-centered Monkhorst–Pack **k**-point mesh of $3 \times 3 \times 1$ ($18 \times 18 \times 1$) for monolayers and $3 \times 1 \times 1$ ($18 \times 1 \times 1$) for nanoribbons for optimization (density of states) calculations. Dispersion interactions were included using Grimme's DFT-D2 method [41], accounting for van der Waals forces to accurately describe interatomic interactions in porous carbon frameworks.

To evaluate the dynamical stability of β-naphthyne, phonon dispersion calculations were performed using density functional perturbation theory (DFPT) as implemented in the Phonopy package [42]. Additionally, *ab initio* molecular dynamics (AIMD) simulations were conducted at 300 K for 5 ps in the NVT ensemble, employing the Nosé-Hoover thermostat [43,44] to assess its thermal robustness.

The optical properties were investigated through calculations of the frequency-dependent dielectric function, from which absorption coefficients and reflectance spectra were derived [45], providing insight into the potential optoelectronic applications of β-naphthyne.

The energetic stability of β-naphthyne was analyzed by its cohesive energy (E_{coh}):

$$E_{coh} = \frac{E_{\beta\text{-naphthyne}} - \sum_i n_i E_i}{\sum_i n_i}, \quad (1)$$

where $E_{\beta\text{-naphthyne}}$ is the total energy of the structure, E_i represents the energy of isolated C atoms, and n_i is the atom count of each element. The same approach was used to obtain the E_{coh} for other 2D structures discussed in this work.

To analyze the vibrational properties of β-naphthyne, the coupled perturbed HF/Kohn–Sham algorithm [46] implemented in the computational package CRYSTAL17 [47] was used. The calculations in CRYSTAL17 were performed using triple-zeta valence with polarization (TZVP) basis set [48] together with the B3LYP functional. The structure was optimized by checking the root mean square (RMS) and the absolute value of the largest component of both the gradients and the estimated displacements. The convergence criteria used in the optimization for RMS and the largest component for gradient (0.00030 a.u. and 0.00045 a.u.) and displacement (0.00120 a.u. and 0.00180 a.u.), respectively. The reciprocal space was sampled using Pack-Monkhost and Gilat nets with sublattice and a shrinking factor of 12.

3. Results

3.1. Structure and stability

β-naphthyne is characterized by a rectangular conventional unit cell that belongs to the *Cmm* (no. 65) space group, with lattice parameters $a = 10.74$ Å and $b = 11.72$ Å (see Fig. 1a). The primitive cell comprises lattice parameters $a = b = 7.82$ Å, $\alpha = \beta = 90°$, and $\gamma = 93.17°$. The conventional unit cell consists of five crystallographically distinct carbon atoms located in C1 (0.764, 0.378, 0.500), C2 (0.359, 0.181, 0.500), C3 (0.566, 0.282, 0.500), C4 (0.367, 0.392, 0.500), and C5 (0.932, 0.000, 0.500). This structure forms a 2D carbon framework comprising 6–8 carbon-membered rings, where octagonal rings interconnect naphthyl fragments. For comparison purposes, Table 1 details the lattice parameters (a, b, $\alpha = \beta$, and γ), space group (SPG), band gap energy (E_{gap}), and cohesive energy (E_{coh}) for several carbon monolayers. The comparison shows that the cohesive energy (E_{coh}) of β-naphthyne (−7.25 eV/atom) is competitive with other 2D carbon allotropes, being close to that of T-graphene (−7.45 eV/atom) and graphenylene (−7.33 eV/atom), but lower than that of pure graphene (−8.02 eV/atom). The E_{coh} reflects the energy required to disassemble a solid into isolated atoms, serving as a key indicator of the structural stability of the material. Therefore, while β-naphthyne shows slightly weaker cohesion than graphene, its value remains sufficiently high to imply a stable 2D structure.

To evaluate the dynamical stability of β-naphthyne, the phonon dispersion was computed along the high-symmetry paths of the Brillouin zone, as depicted in Fig. 1b. The dispersion confirms the absence of imaginary frequencies, indicating that the material is dynamically stable. At the Γ-point, three acoustic modes with a characteristic linear behavior. Several phonon branches remain relatively flat in the 18–25 THz range, suggesting low group velocity and localized vibrational modes. In contrast, the bands display quadratic dispersion in the 25–35 THz range, indicating high phononic mobility. Finally, vibrational modes with flat characteristics above 60 THz correspond to the sp-hybridized bonds in β-naphthyne, a common feature in graphyne-like systems [55].

One critical aspect in assessing the viability of novel 2D materials is their thermal stability under ambient conditions. In this way, AIMD simulations were performed at 300 K for a total duration time of 4 ps. Fig. 2a depicts the evolution of the total energy fluctuations during the simulation, along with the final atomic configuration (Fig. 2b).

The total energy stabilizes after the first picosecond of the simulation. After this phase, energy fluctuations remain minimal, consistently within a range of less than 1 eV, indicating structural robustness. The absence of significant deviations suggests that no phase transitions or reconstruction events occur during the simulation, further supporting the stability of the material at room temperature. The final atomic configuration, presented in Fig. 2b, further corroborates this observation. The top and side views reveal that the structural integrity of β-naphthyne is preserved, with only minor out-of-plane distortions emerging.

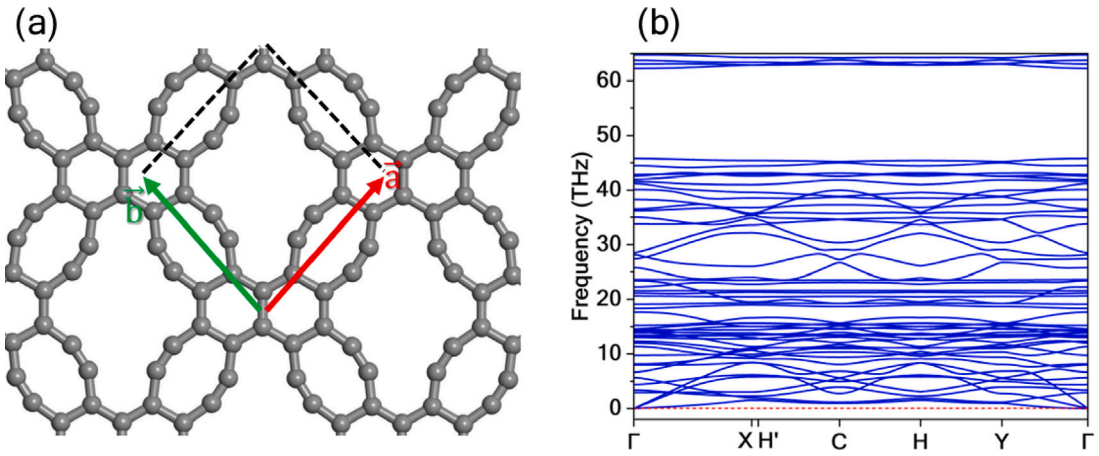

Fig. 1. (a) Top view of the optimized β-naphthyne unit cell (primitive lattice vectors $a = b = 7.82$ Å); (b) phonon-dispersion along the high-symmetry directions of the Brillouin zone.

Table 1
Lattice parameters (a and b in Å, $\alpha = \beta$, and γ in degrees), space group (SPG), band gap energy (E_{gap}) in eV, and cohesive energy (E_{coh}) in eV/atom obtained for β-naphthyne and other relevant 2D carbon allotropes at DFT/GGA-PBE level. The values reported in this table were calculated in this study.

	a	b	$\alpha = \beta$	γ	SPG	E_{gap}	E_{coh}
β-naphthyne (this work)	10.74	11.43	90	90	Cmm (65)	Metallic	−7.25
T-graphene [49]	3.45	3.45	90	90	$P4/mmm$ (123)	Metallic	−7.45
Twin-graphene [50]	6.14	6.14	90	120	$P6/mmm$ (191)	0.73	−7.08
PHE-graphene [51]	5.73	5.73	90	120	$P\bar{6}m2$ (187)	Metallic	−7.56
Penta-graphene [21]	3.64	3.64	90	90	$P42_1m$ (113)	2.19	−7.13
Graphyine [52]	9.46	9.46	90	120	$P6/mmm$ (191)	Metallic	−7.20
Graphenyldiene [28]	9.32	9.32	90	120	$P6/mmm$ (191)	0.78	−6.92
Graphenylene [27,53]	6.77	6.77	90	120	$P6/mmm$ (191)	0.04	−7.33
Biphenylene [19]	3.80	4.50	90	90	$Pmmm$ (47)	Metallic	−7.47
Graphene [54]	2.47	2.47	90	120	$P6/mmm$ (191)	Metallic	−8.02

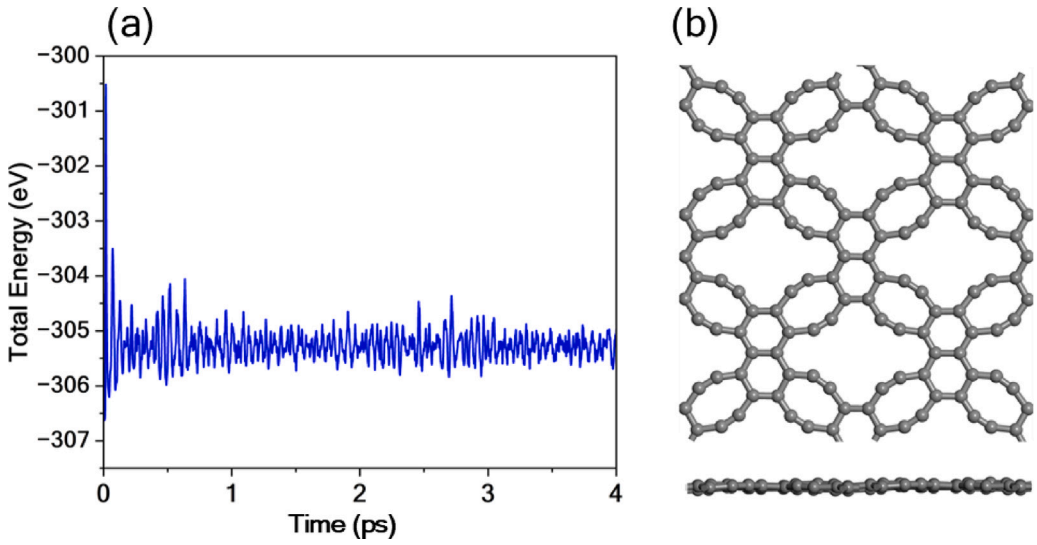

Fig. 2. (a) Evolution of the total energy at 300 K over a 4 ps AIMD run; (b) final atomic configuration (top and side views) after the simulation.

3.2. Electronic analysis

We performed a detailed analysis of the band structure to investigate the electronic properties of β-naphthyne. The results, depicted in Fig. 3, confirm that β-naphthyne exhibits metallic behavior with a band partially occupied crossing the Fermi level (E_F) closer to the Γ point. The states that compose this band can act as acceptor states, receiving the electronic density, which can be useful for an effective interaction with metal adatoms. In the valence band (VB), one can observe that the bands exhibit high dispersion, with several crossings, indicating a strong coupling between the electronic states. On the other hand, when the conduction band (CB) is analyzed, the lowest energy band touches E_F two times at the points H' and H. This band presents a high dispersion, around 2 eV.

The projected density of states (PDOS) analysis provides a more detailed understanding of the electronic structure, shown in Fig. 4, which decomposes the total density of states into atomic orbital contributions. The VB and CB predominantly comprise p orbitals, with the p_y states

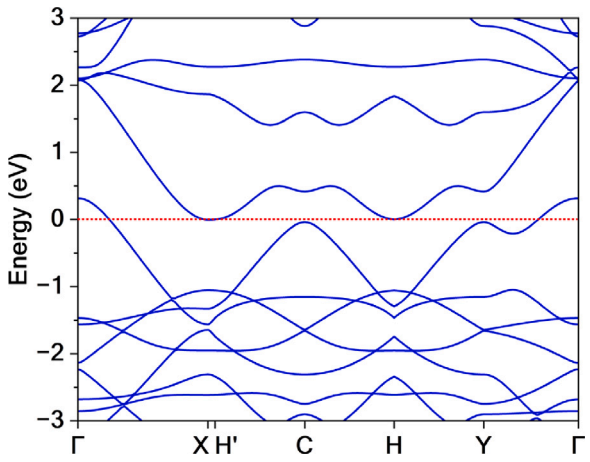

Fig. 3. Electronic band structure of β-naphthyne along the principal Brillouin-zone paths; the red dashed line marks the Fermi level (E_F) (set to 0 eV).

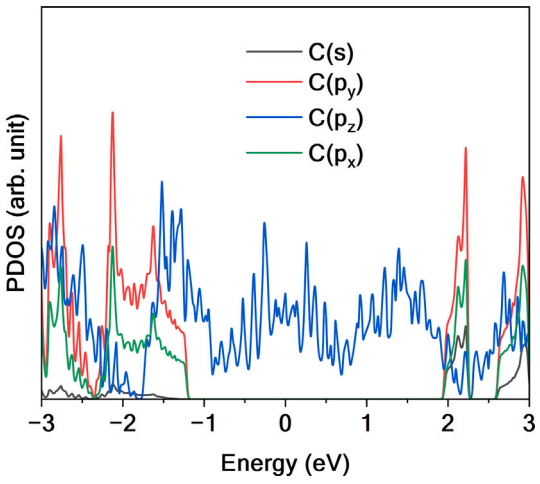

Fig. 4. Orbital-resolved projected density of states (PDOS) for β-naphthyne.

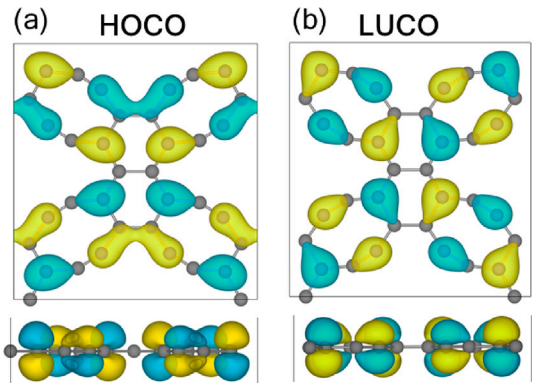

Fig. 5. Real-space distribution of (a) the highest occupied crystalline orbital (HOCO) and (b) the lowest unoccupied crystalline orbital (LUCO) of β-naphthyne.

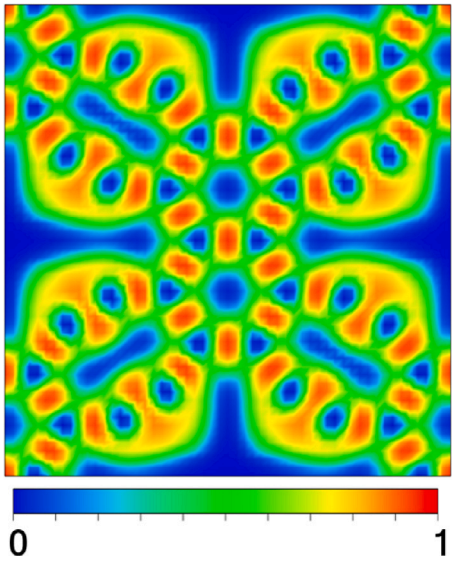

Fig. 6. Electron localization function (ELF) of β-naphthyne.

contributing most significantly, closely followed by the p_x states. The similar energy distribution profiles of the p_y and p_x orbitals suggest a strong orbital coupling in these energy regions. However, near the E_F, it becomes evident that only the p_z orbitals contribute, indicating a pronounced π-character in this energy range.

To further investigate the electronic properties of β-naphthyne, we analyzed the spatial distribution of its frontier crystalline orbitals, specifically the highest occupied crystalline orbital (HOCO) and the lowest unoccupied crystalline orbital (LUCO), as shown in Fig. 5. Fig. 5a illustrates HOCO, which is predominantly composed of π-type orbitals located on the naphthyl units. The electron density is highly delocalized across the hexagonal rings, indicating a strong conjugation network. The side view further confirms the planarity of the electronic distribution, reinforcing the 2D nature of the conduction pathways.

Fig. 5b shows the LUCO, which also exhibits a π-character, but with electron density more prominently localized around the octagonal rings. This spatial separation between the HOCO and LUCO suggests a moderate charge transfer character, which could influence optical excitations and recombination rates. The LUCO distribution indicates that electron transport might be primarily facilitated through the octagonal framework, complementing the hole conduction pathways of the HOCO.

The distinct spatial location of HOCO and LUCO further supports the metallic nature of β-naphthyne, as both orbitals maintain a significant density near the E_F. The overlap of these orbitals could also contribute to strong optical absorption, suggesting potential applications in photodetectors and optoelectronic devices, as will be discussed later.

To gain a deeper understanding of the charge distribution and bonding nature of β-naphthyne, we analyzed its electron localization function (ELF), as shown in Fig. 6. The ELF provides valuable information on the degree of electron localization, where a value of 1 indicates strongly localized electrons (e.g., covalent bonds or lone pairs), a value of 0.5 corresponds to a homogeneous electron gas-like distribution, and a value of 0 represents regions with minimal or no electron density.

In β-naphthyne, the naphthyl fragments exhibit high ELF values, as expected due to the sp^2 hybridization. In contrast, the octagonal rings exhibit lower ELF values, indicating greater electron delocalization than the naphthyl units. This behavior can be attributed to sp-hybridized bonds, which result in a more diffuse electron density along the in-plane bonds.

The ELF map further supports the conclusion that β-naphthyne exhibits a highly delocalized electronic structure, with distinct regions contributing to different transport properties. The bond interactions within the naphthyl and octagonal rings, i.e., the combination of sp and sp^2 hybridizations, create a unique electronic environment, making this material a promising candidate for nanoelectronic and optoelectronic applications, where controlled charge delocalization and transport are essential.

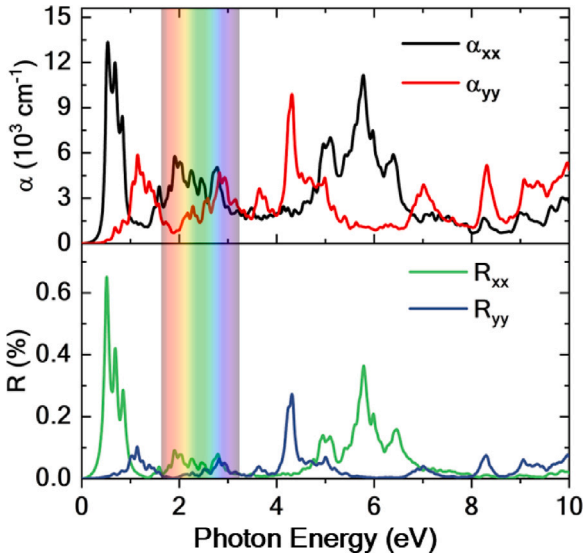

Fig. 7. Optical response of β-naphthyne: (top) absorption coefficient (α) for light polarized along x (black) and y (red); (bottom) reflectance (R) for the same polarization directions, x (green) and y (blue).

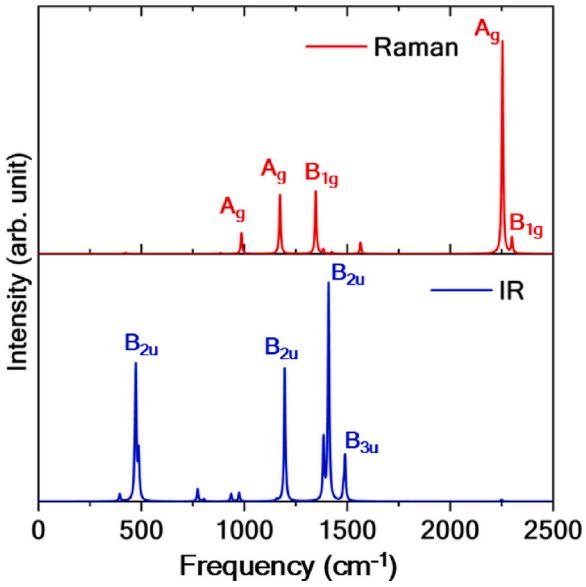

Fig. 8. Calculated vibrational spectra of β-naphthyne: (top) Raman spectrum and (bottom) infrared spectrum.

3.3. Optical properties

To address the optical properties of β-naphthyne, we calculated its absorption coefficient (α) and reflectance (R), as illustrated in Fig. 7. The visible light range is highlighted in the figure to facilitate the identification of its transparency and absorption characteristics.

β-Naphthyne exhibits strong absorption in the IR region, with the absorption coefficient reaching approximately 14×10^3 cm^{-1} for the x component. This result suggests that the material could be well-suited for IR photodetectors and thermal shielding applications. Additionally, the y component shows noticeable absorption in the near-IR range, further reinforcing its potential for IR-active optoelectronic devices.

The absorption onset for the x-component is observed near 0.4 eV, which corresponds to a wavelength of approximately 3.1 μm. This places it at the boundary between the short-wave infrared (SWIR, 1.4–3 μ m) and the mid-wave infrared (MWIR, 3–5 μ m) regions. These spectral ranges are relevant for various commercial IR devices such as gas sensors [56] and environmental monitoring [57] systems, indicating that β-naphthyne could be a promising candidate for MWIR photodetection technologies.

The material displays relatively low absorption in the visible spectrum, with the maximum absorption coefficient reaching 6×10^3 cm^{-1} between the red and orange spectral regions for the x component. This trend suggests that β-naphthyl is mainly transparent to visible light, making it a promising candidate for transparent conducting films or low-energy-loss optical coatings. The reflectance in this range remains minimal. β-naphthyne exhibits strong absorption peaks in the UV region, with significant transitions occurring around 4.5 eV (y component) and 6 eV (x component).

3.4. Vibrational properties

Vibrational spectroscopy provides essential insights into the bonding nature and structural integrity of materials. To assess the phonon behavior of β-naphthyne, we computed both the Raman and IR spectra, as shown in Fig. 8. These spectra allow us to distinguish between Raman-active and IR-active vibrational modes, shedding light on the symmetry and electronic environment of atomic vibrations in the material.

The vibrational modes of β-naphthyne can be represented by $\Gamma_{vib} = 5B_{1u} + 9B_{2u} + 9B_{3u} + 4B_{2g} + 4A_u + 5B_{3g} + 9B_{1g} + 9A_g$. Between these modes, three are acoustic ($B_{1u} + B_{2u} + B_{3u}$), four are silent ($4A_u$), 23 are IR-active ($5B_{1u} + 9B_{2u} + 9B_{3u}$), and 27 are Raman-active ($4B_{2g} + 5B_{3g} + 9B_{1g} + 9A_g$).

Analyzing the Raman spectrum (Fig. 8, top panel) reveals several distinct peaks, with the most intense modes Ag and B_{1g} occurring at low and intermediate frequencies. Four prominent bands are visible at 985 cm^{-1} (A_g), 1172 cm^{-1} (A_g), 1383 cm^{-1} (B_{1g}), and 2253 cm^{-1} (A_g). Strong A_g symmetric modes suggest collective in-plane stretching and breathing vibrations of the carbon framework.

However, by verifying the IR spectrum (Fig. 8, bottom panel), several intense peaks associated with asymmetric stretching and bending modes are shown. Four intense bands are noticed at 472 cm^{-1} (B_{2u}), 1196 cm^{-1} (B_{2u}), 1409 cm^{-1} (B_{2u}), and 1489 cm^{-1} (B_{3u}) are observed. The B_{2u} and B_{3u} indicate dipole-active vibrations arising from charge asymmetry within the structure. The strongest IR peak, located around 1500 cm^{-1}, is related to C–C stretching motions similar to those observed in other 2D carbon-based materials [58,59]. The presence of multiple low-frequency peaks suggests the existence of out-of-plane bending and deformation modes.

3.5. Mechanical properties

The mechanical properties of β-naphthyne were assessed by calculating its elastic constants, which are crucial to determining the material's structural stability and mechanical response. The obtained values for the independent elastic constants are C_{11} = 169.10 N/m, C_{22} = 173.64 N/m, C_{12} = 42.68 N/m, C_{16} = −22.32 N/m, C_{26} = −17.49 N/m, and C_{66} = 20.98 N/m. According to the Born-Huang stability criteria [60], the mechanical stability of 2D oblique systems is ensured if $C_{11} > 0$, $C_{11}C_{22} > C_{12}^2$, and $\det(C_{ij}) > 0$. Substituting the calculated values, these conditions are satisfied. Therefore, we confirm that the β-naphthyne structure is mechanically stable under small deformations.

One can note that Young's modulus (Y), which quantifies the material's resistance to uniaxial deformation, exhibits strong anisotropy. As shown in Fig. 9a, Y reaches a maximum of 165.88 N/m along one crystallographic direction and a minimum of 43.71 N/m in the perpendicular direction, resulting in an anisotropy ratio of 3.79. This trend suggests that the material's stiffness is strongly dependent on the applied strain direction [61]. The maximum Young's modulus

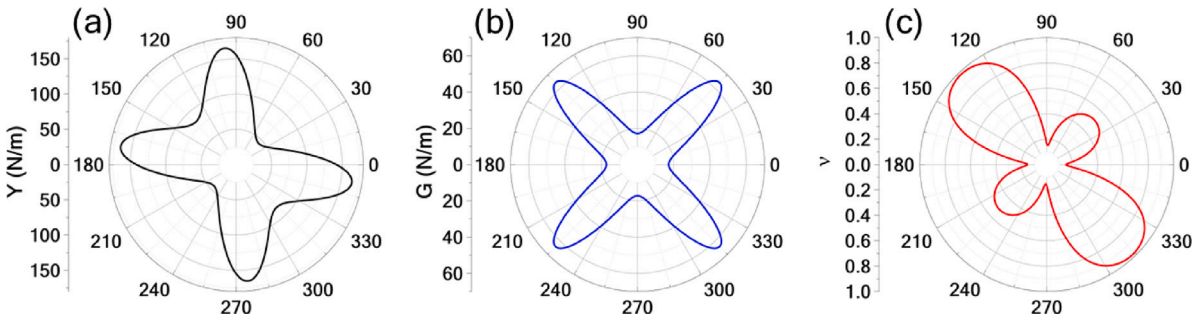

Fig. 9. Polar plots of the in-plane mechanical properties of β-naphthyne: (a) Young's modulus (Y), (b) shear modulus (G), and (c) Poisson's ratio (ν).

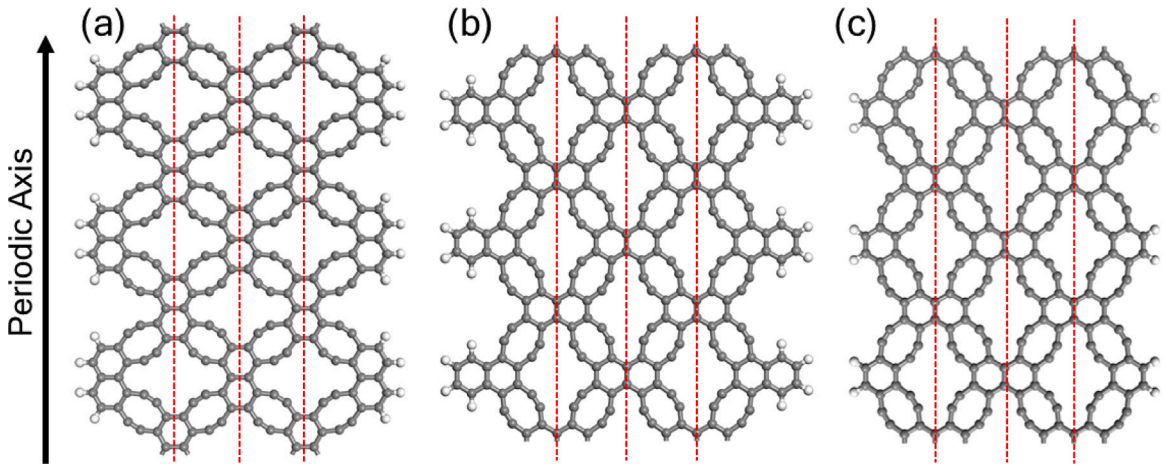

Fig. 10. Schematic representation of the 1D structures of β-naphthyne nanoribbons. (a) Zigzag nanoribbon (ZNNR), (b) armchair nanoribbon with double hexagon edges (ANNR-hh), and (c) armchair nanoribbon with single hexagon edges (ANNR-h).

Table 2
Maximum and minimum values of Young's modulus (Y_{max}, Y_{min}) in N/m, Poisson ratio (ν_{max}, ν_{min}), and Shear modulus (G_{max}, G_{min}) in N/m for β-naphthyne and other carbon monolayers. The values reported in this table were calculated in this study.

	Y_{max}/Y_{min}	ν_{max}/ν_{min}	G_{max}/G_{min}
β-naphthyne	165.88/43.71	0.98/0.15	63.94/17.17
PHE-graphene	262.29/262.29	0.26/0.26	103.91/103.91
Graphenylene	209.02/209.02	0.27/0.27	82.11/82.11
Graphene	345.42/345.42	0.17/0.17	147.60/147.60
Graphenyldiene	122.47/122.47	0.35/0.35	45.29/45.29
Penta-graphene	271.81/266.67	−0.08/−0.10	151.21/144.98
T-graphene	293.90/148.02	0.16/0.58	126.57/148.02
Graphyne	123.59/123.59	0.45/0.45	42.63/42.63

of β-naphthyne surpasses that of graphenyldiene (122.47 N/m) and graphyne (123.59 N/m) (refer to Table 2).

The shear modulus (G), which describes the resistance to shear deformations, also demonstrates notable directional variation. Fig. 9b depicts that G varies from 63.93 N/m to 17.17 N/m, corresponding to an anisotropy ratio of 3.73. Interestingly, the maximum shear modulus (G_{max} exceeds that of graphenyldiene (45.29 N/m) and graphyne (42.63 N/m), suggesting that β-naphthyne resists shear forces more effectively than other related 2D carbon materials. The Poisson's ratio (ν), shown in Fig. 9c, exhibits the highest degree of anisotropy, ranging from 0.98 to 0.15, with an anisotropy ratio of 6.48. This extreme variation indicates that β-naphthyne's ability to contract in one direction when stretched in another highly depends on the strain orientation. This wide range of mechanical properties in β-naphthyne is comparable to that of several anisotropic materials ever reported, such as T-graphene [62], Ographene [63], and 2D MoO_3 [64], and Tetrahex Carbon [65]. Furthermore, this feature also highlights its potential for applications that require directional mechanical responses, such as mechanical metamaterials [66], strain-sensitive output devices [67,68], and flexible electronics [69].

3.6. One-dimensional (1D) structures

We now turn our attention to nanoribbons derived from β-naphthyne. Due to their rectangular lattice, the nanoribbons were generated by exploring the cutting directions of the armchair (y or b) and zigzag (x or a). It is worth noting that experimental control over edge terminations in atomically precise nanoribbons remains a challenge. Techniques such as bottom-up synthesis or post-growth chemical functionalization may be necessary to stabilize the edges of well-defined nanoribbons and preserve their electronic properties [70–72].

The armchair and zigzag β-naphthyne nanoribbons are referred to as ANNR and ZNNR, respectively. For ZNNR, we considered a single type of edge in the non-periodic direction, consisting of two hexagons, as illustrated in Fig. 10a. In the case of ANNRs, two edge terminations were examined: one with two hexagons (hh) (Fig. 10b) and another with a single hexagon (h) (Fig. 10c), labeled ANNR-hh and ANNR-h, respectively. The chosen nanoribbon width spans three naphthyl groups. This methodology is in agreement with the approach adopted by Paz et al. [32] in their investigation of the 1D structures of β-naphthylene. Note that β-naphthyne nanoribbons did not show reconstructions or bond breaks in optimization. In addition, the planarity of 2D β-naphthyne was maintained.

To explore the electronic properties of the β-naphthyne 1D structures, we calculated the band structures for ZNNR, ANNR-h, and ANNR-hh, as depicted in Fig. 11. The ZNNR retains a metallic character, mirroring its 2D counterpart. However, a remarkable characteristic emerges with a Dirac cone positioned closer to the Γ point. In contrast,

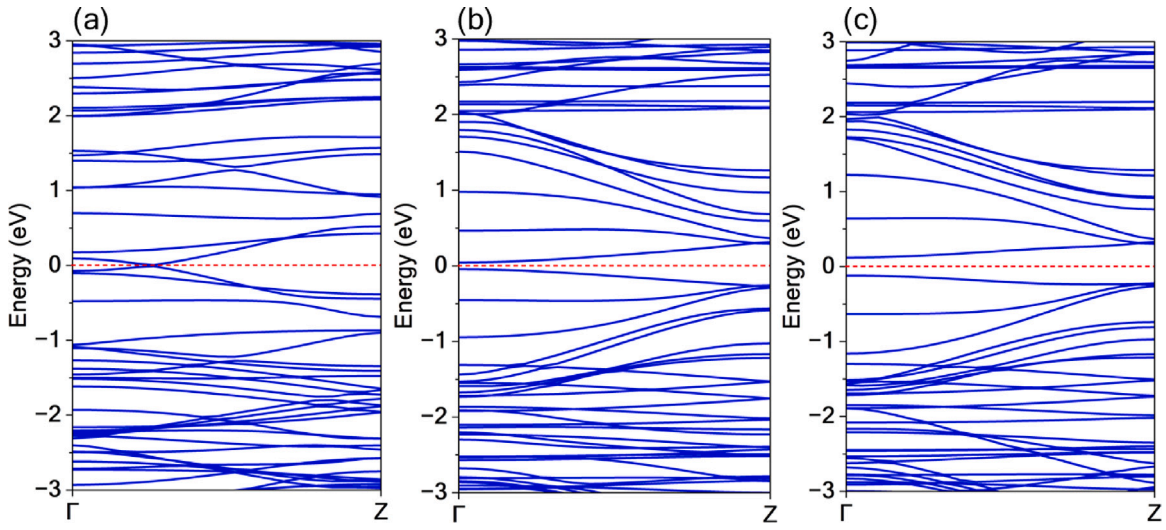

Fig. 11. Electronic band structures of β-naphthyne nanoribbons: (a) zigzag-edge nanoribbon (ZNNR), (b) armchair-edge nanoribbon with hollow–hollow edges (ANNR-*hh*), and (c) armchair-edge nanoribbon with hollow edges (ANNR-*h*); the red dashed line denotes the Fermi level (E_F).

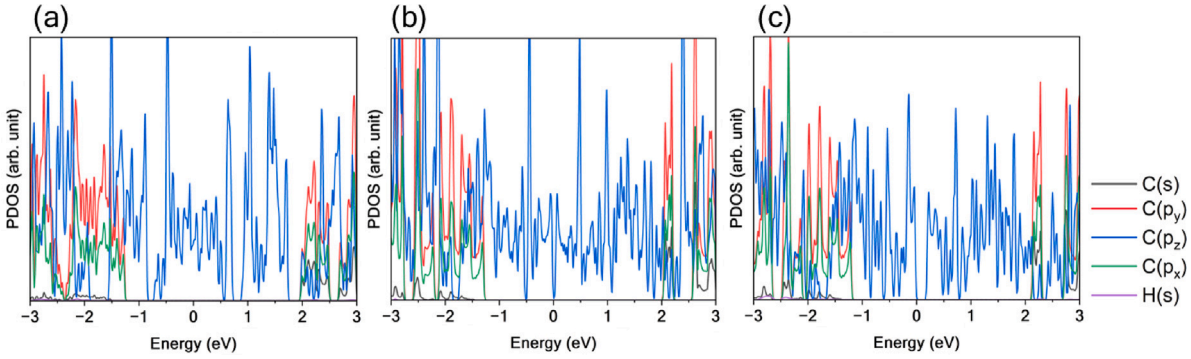

Fig. 12. Projected density of states (PDOS) for β-naphthyne nanoribbons: (a) ZNNR, (b) ANNR-*hh*, and (c) ANNR-*h*.

the ANNR-*hh* and ANNR-*h* structures reveal a transition from metallic to semiconducting behavior, with direct band gaps at the Γ point of 0.08 eV and 0.24 eV, respectively. This band gap opening can be attributed to the edge-induced symmetry-breaking and quantum confinement effects inherent to the reduced dimensionality.

To verify the composition of the electronic states of the β-naphthyne nanoribbons, the projected density of states (PDOS) was calculated, as shown in Fig. 12. The general features closely resemble those of the 2D counterpart, such as the prominent contribution of p_y and p_x states at the lower and higher energies of the valence band (VB) and conduction band (CB), respectively. Around the Fermi level (E_F), the p_z states dominate entirely, with no significant contributions from other orbitals. Furthermore, hydrogen states do not show relevant influence across the evaluated energy range.

For ZNNR (Fig. 12a), despite the presence of a Dirac cone, the PDOS reveals a non-zero density of states at the Fermi level. This finite DOS arises from the low dispersion of bands near the Dirac point, causing an accumulation of electronic states around E_F, preventing the DOS from vanishing completely. In the cases of ANNR-*hh* (Fig. 12b) and ANNR-*h* (Fig. 12c), a noticeable accumulation of states at the band edges is observed, accompanied by an abrupt drop in the DOS at these regions, characteristic of highly correlated electronic states.

4. Conclusion

In this work, we explore the structural, electronic, mechanical and optical properties of a novel porous 2D carbon allotrope, β-naphthyne, using first-principles calculations. Our results confirmed its stability, with phonon dispersion and *ab initio* molecular dynamics (AIMD) simulations indicating a robust framework.

The electronic band structure revealed that β-naphthyne exhibits metallic behavior, with strong π-character for the states in the band edges. Mechanical analysis highlighted its strong anisotropy, showing a significant directional dependence on Young's modulus, shear modulus, and Poisson's ratio. This mechanical anisotropy surpasses that of previously studied 2D carbon materials, positioning β-naphthyne as a promising candidate for strain engineering applications.

Optical investigations demonstrated that β-naphthyne exhibits strong IR absorption, moderate interaction within the visible spectrum, and pronounced UV absorption peaks, suggesting its potential for optoelectronic and photonic technologies. Furthermore, the Raman and IR spectra provided distinctive vibrational fingerprints, providing a reliable reference for future experimental validation.

We further examine the electronic properties of 1D β-naphthyne nanoribbons. Although ZNNR retained the metallic character of its 2D counterpart, ANNR-*h* and ANNR-*hh* showed a transition from metallic to semiconducting behavior, with direct band gaps of 0.08 and 0.24 eV, respectively. These findings underscore the tunable electronic properties of β-naphthyne, driven by dimensionality reduction and edge geometry, broadening its potential for nanoelectronic applications.

CRediT authorship contribution statement

José A.S. Laranjeira: Writing – review & editing, Writing – original draft, Methodology, Formal analysis, Conceptualization. **K.A.L. Lima:**

Writing – review & editing, Writing – original draft, Methodology, Investigation, Formal analysis, Conceptualization. **Nicolas F. Martins:** Writing – review & editing, Writing – original draft, Methodology, Investigation, Formal analysis, Conceptualization. **Marcelo L.P. Junior:** Writing – review & editing, Writing – original draft, Methodology, Formal analysis, Conceptualization. **L.A. Ribeiro Junior:** Writing – review & editing, Writing – original draft, Methodology, Formal analysis, Conceptualization. **Julio R. Sambrano:** Writing – review & editing, Writing – original draft, Methodology, Formal analysis, Conceptualization.

Declaration of competing interest

The authors declare that they have no known competing financial interests or personal relationships that could have appeared to influence the work reported in this paper.

Acknowledgments

This work was supported by the Brazilian funding agencies Fundação de Amparo à Pesquisa do Estado de São Paulo - FAPESP (grant no. 2022/03959-6, 2022/14576-0, 2020/01144-0, 2024/05087-1, and 2022/16509-9), and National Council for Scientific, Technological Development - CNPq, Brazil (grant no. 307213/2021–8). L.A.R.J. acknowledges the financial support from FAP-DF grants 00193.00001808/2022-71 and 00193-00001857/2023-95, FAPDF-PRONEM grant 00193.00001247/2021-20, PDPG-FAPDF-CAPES Centro-Oeste 00193-00000867/2024-94, and CNPq grants 350176/2022-1 and 167745/2023-9.

Data availability

Data will be made available on request.

References

[1] Santosh K. Tiwari, Vijay Kumar, Andrzej Huczko, R. Oraon, A. De Adhikari, G.C. Nayak, Magical allotropes of carbon: prospects and applications, Crit. Rev. Solid State Mater. Sci. 41 (4) (2016) 257–317.

[2] Salisu Nasir, Mohd Zobir Hussein, Zulkarnain Zainal, Nor Azah Yusof, Carbon-based nanomaterials/allotropes: A glimpse of their synthesis, properties and some applications, Materials 11 (2) (2018) 295.

[3] Susmita Jana, Arka Bandyopadhyay, Sujoy Datta, Debaprem Bhattacharya, Debnarayan Jana, Emerging properties of carbon based 2D material beyond graphene, J. Phys.: Condens. Matter. 34 (5) (2021) 053001.

[4] Panpan Li, Wenhao He, Pengfei Ju, Li Ji, Xiaohong Liu, Fan Wu, Zhibin Lu, Hongxuan Li, Lei Chen, Jingzhou Liu, et al., Acquisition of molecular rolling lubrication by self-curling of graphite nanosheet at cryogenic temperature, Nat. Commun. 15 (1) (2024) 5747.

[5] Xiong Zhang, Haitao Zhang, Chen Li, Kai Wang, Xianzhong Sun, Yanwei Ma, Recent advances in porous graphene materials for supercapacitor applications, Rsc Adv. 4 (86) (2014) 45862–45884.

[6] Ning Yang, Haonan Li, Xiao Lin, Stella Georgiadou, Liang Hong, Zhaohua Wang, Fan He, Zhifu Qi, Wen-Feng Lin, Catalytic electrode comprising a gas diffusion layer and bubble-involved mass transfer in anion exchange membrane water electrolysis: A critical review and perspectives, J. Energy Chem. 105 (2025) 669–701.

[7] Mengcheng Wu, Wanying Zheng, Xi Hu, Feiyang Zhan, Qingqing He, Huayu Wang, Qichun Zhang, Lingyun Chen, Exploring 2D energy storage materials: Advances in structure, synthesis, optimization strategies, and applications for monovalent and multivalent metal-ion hybrid capacitors, Small 18 (50) (2022) 2205101.

[8] Mingguang Wu, Jiaqin Liao, Lingxiao Yu, Ruitao Lv, Peng Li, Wenping Sun, Rou Tan, Xiaochuan Duan, Lei Zhang, Fang Li, et al., 2020 Roadmap on carbon materials for energy storage and conversion, Chemistry–Asian J. 15 (7) (2020) 995–1013.

[9] Cong Wang, Yunxia Chen, Unsupervised dynamic prognostics for abnormal degradation of lithium-ion battery, Appl. Energy 365 (2024) 123280.

[10] PengTao Xu, JiXiang Yang, KeSai Wang, Zhen Zhou, PanWen Shen, Porous graphene: Properties, preparation, and potential applications, Chin. Sci. Bull. 57 (2012) 2948–2955.

[11] Haibo Huang, Haodong Shi, Pratteek Das, Jieqiong Qin, Yaguang Li, Xiao Wang, Feng Su, Pengchao Wen, Suyuan Li, Pengfei Lu, et al., The chemistry and promising applications of graphene and porous graphene materials, Adv. Funct. Mater. 30 (41) (2020) 1909035.

[12] Albert Guirguis, James W. Maina, Xiwang Zhang, Luke C. Henderson, Lingxue Kong, Hokyong Shon, Ludovic F. Dumée, Applications of nano-porous graphene materials–critical review on performance and challenges, Mater. Horizons 7 (5) (2020) 1218–1245.

[13] Ding Zhou, Yi Cui, Pei-Wen Xiao, Mei-Yang Jiang, Bao-Hang Han, A general and scalable synthesis approach to porous graphene, Nat. Commun. 5 (1) (2014) 4716.

[14] Guan Huang, Lichuan Zhang, Shibing Chu, Yuee Xie, Yuanping Chen, A highly ductile carbon material made of triangle rings: A study of machine learning, Appl. Phys. Lett. 124 (4) (2024) 043103.

[15] Yan Fang, Yuxin Liu, Lu Qi, Yurui Xue, Yuliang Li, 2D graphdiyne: an emerging carbon material, Chem. Soc. Rev. 51 (7) (2022) 2681–2709.

[16] Alexandre Cavalheiro Dias, Carlos Derli Almeida Cornelio, Mauricio Jeomar Piotrowski, Luiz Antonio Ribeiro Juunior, Carlos Maciel de Oliveira Bastos, Celso Ricardo Caldeira Reego, Diego Guedes-Sobrinho, Can 2D carbon allotropes be used as photovoltaic absorbers in solar harvesting devices? ACS Appl. Energy Mater. 7 (19) (2024) 8572–8582.

[17] Boris I. Kharisov, Oxana V. Kharissova, Lucy T. González, Yolanda Peña Méndez, Igor E. Uflyand, Naveen Kulkarni, Density function theory predicted carbon allotropes: Recent developments, ChemistrySelect 8 (24) (2023) e202301567.

[18] Xin Gao, Huibiao Liu, Dan Wang, Jin Zhang, Graphdiyne: synthesis, properties, and applications, Chem. Soc. Rev. 48 (3) (2019) 908–936.

[19] Qitang Fan, Linghao Yan, Matthias W. Tripp, Ondřej Krejčí, Stavrina Dimosthenous, Stefan R. Kachel, Mengyi Chen, Adam S. Foster, Ulrich Koert, Peter Liljeroth, et al., Biphenylene network: A nonbenzenoid carbon allotrope, Science 372 (6544) (2021) 852–856.

[20] Yu Liu, Gang Wang, Qingsong Huang, Liwei Guo, Xiaolong Chen, Structural and electronic properties of T graphene: A two-dimensional<? format?> carbon allotrope with tetrarings, Phys. Rev. Lett. 108 (22) (2012) 225505.

[21] Shunhong Zhang, Jian Zhou, Qian Wang, Xiaoshuang Chen, Yoshiyuki Kawazoe, Puru Jena, Penta-graphene: A new carbon allotrope, Proc. Natl. Acad. Sci. 112 (8) (2015) 2372–2377.

[22] Raphael M. Tromer, Marcelo L. Pereira Junior, Kleuton A. L. Lima, Alexandre F. Fonseca, Luciano R. da Silva, Douglas S. Galvão, Luiz A. Ribeiro Junior, Mechanical, electronic, and optical properties of 8-16-4 graphyne: A 2d carbon allotrope with dirac cones, J. Phys. Chem. C 127 (25) (2023) 12226–12234.

[23] M.L. Pereira Júnior, Wiliam Ferreira da Cunha, William Ferreira Giozza, Rafael Timoteo de Sousa Junior, L.A. Ribeiro Junior, Irida-graphene: A new 2d carbon allotrope, FlatChem 37 (2023) 100469.

[24] Roya Majidi, Irida-graphyne: A promising material for optoelectronic applications, Mater. Today Commun. 38 (2024) 107641.

[25] Kleuton A.L. Lima, Rodrigo A.F. Alves, Daniel A. da Silva, Fábio L.L. Mendonça, Marcelo L. Pereira, Luiz A. Ribeiro, TH-graphyne: a new porous bidimensional carbon allotrope, Phys. Chem. Chem. Phys. (2025).

[26] K.A.L. Lima, Fábio Ferreira Monteiro, E.J.A. Santos, R.A.F. Alves, William Ferreira Giozza, L.A. Ribeiro Junior, Dodecanophene: A novel 2D carbon allotrope with untunable metallic behavior under stress, Mater. Today Commun. 40 (2024) 109455.

[27] Qi Song, Bing Wang, Ke Deng, Xinliang Feng, Manfred Wagner, Julian D. Gale, Klaus Müllen, Linjie Zhi, Graphenylene, a unique two-dimensional carbon network with nondelocalized cyclohexatriene units, J. Mater. Chem. C 1 (1) (2013) 38–41.

[28] José A.S. Laranjeira, Nicolas F. Martins, Pablo A. Denis, Julio R. Sambrano, Graphenyldiene: A new sp2-graphene-like nanosheet, Carbon Trends 14 (2024) 100321.

[29] Christopher P. Ewels, Xavier Rocquefelte, Harold W. Kroto, Mark J. Rayson, Patrick R. Briddon, Malcolm I. Heggie, Predicting experimentally stable allotropes: Instability of penta-graphene, Proc. Natl. Acad. Sci. 112 (51) (2015) 15609–15612.

[30] Anubhav Jain, Yongwoo Shin, Kristin A. Persson, Computational predictions of energy materials using density functional theory, Nat. Rev. Mater. 1 (1) (2016) 1–13.

[31] Rampi Ramprasad, Rohit Batra, Ghanshyam Pilania, Arun Mannodi-Kanakkithodi, Chiho Kim, Machine learning in materials informatics: recent applications and prospects, Npj Comput. Mater. 3 (1) (2017) 54.

[32] Maria Lúcia Álvares Paz, Aldilene Saraiva-Souza, Vincent Meunier, Eduardo Costa Girão, Naphthylenes: 1D and 2D carbon allotropes based on naphthyl units, Carbon 153 (2019) 792–803.

[33] Harold Hart, Akira Oku, Synthesis and chemistry of octamethylnaphthalene, J. Organic Chem. 37 (26) (1972) 4269–4274.

[34] Dong Han, Junfa Zhu, Surface-assisted fabrication of low-dimensional carbon-based nanoarchitectures, J. Phys.: Condens. Matter. 33 (34) (2021) 343001.

[35] Katsuhiko Ariga, Materials nanoarchitectonics: collaboration between chem, nano and mat, ChemNanoMat 9 (7) (2023) e202300120.

[36] Sylvain Clair, Dimas G. de Oteyza, Controlling a chemical coupling reaction on a surface: tools and strategies for on-surface synthesis, Chem. Rev. 119 (7) (2019) 4717–4776.
[37] Pierre Hohenberg, Walter Kohn, Inhomogeneous electron gas, Phys. Rev. 136 (3B) (1964) B864.
[38] Georg Kresse, Daniel Joubert, From ultrasoft pseudopotentials to the projector augmented-wave method, Phys. Rev. B 59 (3) (1999) 1758.
[39] John P. Perdew, Kieron Burke, Matthias Ernzerhof, Generalized gradient approximation made simple, Phys. Rev. Lett. 77 (18) (1996) 3865.
[40] Georg Kresse, Jürgen Furthmüller, Efficient iterative schemes for ab initio total-energy calculations using a plane-wave basis set, Phys. Rev. B 54 (16) (1996) 11169.
[41] Stefan Grimme, Semiempirical GGA-type density functional constructed with a long-range dispersion correction, J. Comput. Chem. 27 (15) (2006) 1787–1799.
[42] Atsushi Togo, Isao Tanaka, First principles phonon calculations in materials science, Scr. Mater. 108 (2015) 1–5.
[43] Shuichi Nosé, A unified formulation of the constant temperature molecular dynamics methods, J. Chem. Phys. 81 (1) (1984) 511–519.
[44] William G. Hoover, Canonical dynamics: Equilibrium phase-space distributions, Phys. Rev. A 31 (3) (1985) 1695.
[45] Elaine A. Moore, Lesley E. Smart, Optical properties of solids, in: Solid State Chemistry, CRC Press, 2020, pp. 283–314.
[46] Mauro Ferrero, Michel Rérat, Roberto Orlando, Roberto Dovesi, Coupled perturbed hartree-fock for periodic systems: The role of symmetry and related computational aspects, J. Chem. Phys. 128 (1) (2008).
[47] Roberto Dovesi, Roberto Orlando, Bartolomeo Civalleri, Carla Roetti, Victor R. Saunders, Claudio M. Zicovich-Wilson, CRYSTAL: a computational tool for the ab initio study of the electronic properties of crystals, Z. Kristallogr. Cryst. Mater. 220 (5–6) (2005) 571–573.
[48] Daniel Vilela Oliveira, Joachim Laun, Michael F. Peintinger, Thomas Bredow, BSSE-correction scheme for consistent gaussian basis sets of double-and triple-zeta valence with polarization quality for solid-state calculations, J. Comput. Chem. 40 (27) (2019) 2364–2376.
[49] Xian-Lei Sheng, Qing-Bo Yan, Fei Ye, Qing-Rong Zheng, Gang Su, T-carbon: a novel carbon allotrope, Phys. Rev. Lett. 106 (15) (2011) 155703.
[50] Jin-Wu Jiang, Jiantao Leng, Jianxin Li, Zhengrong Guo, Tienchong Chang, Xingming Guo, Tongyi Zhang, Twin graphene: A novel two-dimensional semiconducting carbon allotrope, Carbon 118 (2017) 370–375.
[51] Li Zeng, Yingxiang Cai, Zhihao Xiang, Yu Zhang, Xuechun Xu, A new metallic π-conjugated carbon sheet used for the cathode of li–s batteries, RSC Adv. 9 (1) (2019) 92–98.
[52] Nobuo Narita, Sumiaki Nagai, Shugo Suzuki, Kenji Nakao, Optimized geometries and electronic structures of graphyne and its family, Phys. Rev. B 58 (16) (1998) 11009.
[53] Qi-Shi Du, Pei-Duo Tang, Hua-Lin Huang, Fang-Li Du, Kai Huang, Neng-Zhong Xie, Si-Yu Long, Yan-Ming Li, Jie-Shan Qiu, Ri-Bo Huang, A new type of two-dimensional carbon crystal prepared from 1, 3, 5-trihydroxybenzene, Sci. Rep. 7 (1) (2017) 40796.
[54] Andre K. Geim, Konstantin S. Novoselov, The rise of graphene, Nat. Mater. 6 (3) (2007) 183–191.
[55] Trevor Jenkins, Alexander Martins Silva, Marcos G. Menezes, Timo Thonhauser, Saif Ullah, THD-C sheet: A novel nonbenzenoid carbon allotrope with tetra-, hexa-, and dodeca-membered rings, J. Phys. Chem. C 128 (26) (2024) 10982–10996.
[56] Fang-Xiao Cui, Yue Zhao, An-Jing Wang, Feng-Xiang Ma, Jun Wu, Yang-Yu Li, Da-Cheng Li, Wang-Chao Dong, A multi-spectral thermal gas detection imager using uncooled infrared camera, Optics 3 (4) (2022) 473–482.
[57] Joonsup Shim, Jinha Lim, Inki Kim, Jaeyong Jeong, Bong Ho Kim, Seong Kwang Kim, Dae-Myeong Geum, SangHyeon Kim, Room-temperature waveguide-integrated photodetector using bolometric effect for mid-infrared spectroscopy applications, Light.: Sci. Appl. 14 (1) (2025) 125.
[58] Vincent J. Esposito, Louis J. Allamandola, Christiaan Boersma, Jesse D. Bregman, Ryan C. Fortenberry, Alexandros Maragkoudakis, Pasquale Temi, Anharmonic IR absorption spectra of the prototypical interstellar PAHs phenanthrene, pyrene, and pentacene in their neutral and cation states, Mol. Phys. 122 (7–8) (2024) e2252936.
[59] Sergey M. Kuznetsov, Elena A. Sagitova, Kirill A. Prokhorov, Dmitry I. Mendeleev, Gulnara Yu Nikolaeva, Leila Yu Ustynyuk, Arnulf Materny, Patrice Donfack, Dependence of CC stretching wavenumber on polyene length in degraded polyvinyl chloride: a comparative empirical, classical mechanics, and DFT study, Spectrochim. Acta Part A: Mol. Biomol. Spectrosc. 282 (2022) 121653.
[60] Max Born, On the stability of crystal lattices. I, in: Mathematical Proceedings of the Cambridge Philosophical Society, vol. 36, Cambridge University Press, 1940, pp. 160–172.
[61] Yuhong Zhao, Kexin Liu, Hua Hou, Long-Qing Chen, Role of interfacial energy anisotropy in dendrite orientation in Al-Zn alloys: A phase field study, Mater. Des. 216 (2022) 110555.
[62] Junping Hu, Yu Liu, Ning Liu, Jianwen Li, Chuying Ouyang, Theoretical prediction of T-graphene as a promising alkali-ion battery anode offering ultrahigh capacity, Phys. Chem. Chem. Phys. 22 (6) (2020) 3281–3289.
[63] Shuaiwei Wang, Bingjun Shi, Auxetic ographene: a new 2D Dirac nodal-ring semimetal carbon-based material with a high negative Poisson's ratio, Phys. Chem. Chem. Phys. 24 (2022) 21806–21811.
[64] Sergio Puebla, Roberto D'Agosta, Gabriel Sanchez-Santolino, Riccardo Frisenda, Carmen Munuera, Andres Castellanos-Gomez, In-plane anisotropic optical and mechanical properties of two-dimensional MoO3, Npj 2D Mater. Appl. 5 (1) (2021) 37.
[65] Qun Wei, Guang Yang, Xihong Peng, Auxetic tetrahex carbon with ultrahigh strength and a direct band gap, Phys. Rev. Appl. 13 (2020) 034065.
[66] Pengcheng Jiao, Jochen Mueller, J. Raney, X. Zheng, Amir H. Alavi, Mechanical metamaterials and beyond, Nat. Commun. 14 (2023).
[67] Shidong Ma, Jian Tang, Tao Yan, Z. Pan, Performance of flexible strain sensors with different transition mechanisms: A review, IEEE Sensors J. 22 (2022) 7475–7498.
[68] Junlei Zhang, Yongkang Ye, Zulai Li, Xiang Chen, Weizhang Wang, Guangsheng Huang, Unveiling the mechanical anisotropy and related deformation mechanisms of heterostructured Mg alloy laminate with unique texture feature, J. Alloys Compd. 1010 (2025) 177404.
[69] A.K. Katiyar, Anh Tuan Hoang, Duo Xu, Juyeong Hong, Beom Jin Kim, Seunghyeon Ji, Jong-Hyun Ahn, 2D materials in flexible electronics: Recent advances and future prospectives, Chem. Rev. (2023).
[70] A. Keerthi, B. Radha, Daniel J. Rizzo, Hao Lu, Valentin Diez Cabanes, I. Hou, D. Beljonne, J. Cornil, C. Casiraghi, M. Baumgarten, K. Müllen, A. Narita, Edge functionalization of structurally defined graphene nanoribbons for modulating the self-assembled structures, J. Am. Chem. Soc. 139 (2017) 16454–16457.
[71] A. Narita, Xiao-Ye Wang, Xinliang Feng, K. Müllen, New advances in nanographene chemistry, Chem. Soc. Rev. 44 18 (2015) 6616–6643.
[72] Patrick Han, K. Akagi, F. Federici Canova, H. Mutoh, S. Shiraki, K. Iwaya, P. Weiss, N. Asao, T. Hitosugi, Bottom-up graphene-nanoribbon fabrication reveals chiral edges and enantioselectivity, ACS Nano 8 9 (2014) 9181–9187.